

## Article

# Evaluation and Analysis of the Influence of Rare-Earth Ce on Inclusions in Heavy Rail Steel

Guojun Bai<sup>1,2,3</sup>, Jichun Yang<sup>1,\*</sup> and Wenjing Liang<sup>1,2,3</sup><sup>1</sup> School of Materials and Metallurgy, Inner Mongolia University of Science & Technology, Baotou 014010, China<sup>2</sup> Baotou Steel Mining Co. Ltd., Baotou 014030, China<sup>3</sup> Inner Mongolia Autonomous Region Rare Earth Steel Product R&D Enterprise Key Laboratory, Baotou 014010, China

\* Correspondence: yangjichun1963@163.com

**Abstract:** The effect of rare-earth Ce on the evolution behaviour of inclusions in heavy rail steel was studied. The addition of Ce can significantly reduce the number and size of class A, B, D, and Ds inclusions in the heavy rail steel smelting process. According to the statistical analysis of the size of inclusions in steel, the number and size of A and B inclusions in steel tend to decrease significantly, while D and Ds inclusions disappear. Ce splits the aluminium inclusion into several small-sized inclusions and improves the morphology of the large-size aluminium inclusion, thereby making aggregation and growth difficult while facilitating easy floating and removal. Because the addition of Ce reduces the concentration of S element in steel, MnS inclusions are difficult to grow. The decrease in the number and size of core inclusions required for MnS growth leads to a corresponding decrease in the number and size of MnS inclusions. Meanwhile, the S element also easily gathers on the surface of CaO–MgO–Al<sub>2</sub>O<sub>3</sub>–SiO<sub>2</sub>–CeO inclusions, forming composite inclusions that are more easily removed, thus reducing the quantity and size of MnS inclusions.

**Keywords:** rare earth; heavy rail steel; aluminium-containing inclusions; sulphide inclusion



**Citation:** Bai, G.; Yang, J.; Liang, W. Evaluation and Analysis of the Influence of Rare-Earth Ce on Inclusions in Heavy Rail Steel. *Metals* **2023**, *13*, 614. <https://doi.org/10.3390/met13030614>

Academic Editors: Tomoyoshi Maeno and Roumen Petrov

Received: 31 January 2023

Revised: 13 March 2023

Accepted: 16 March 2023

Published: 19 March 2023



**Copyright:** © 2023 by the authors. Licensee MDPI, Basel, Switzerland. This article is an open access article distributed under the terms and conditions of the Creative Commons Attribution (CC BY) license (<https://creativecommons.org/licenses/by/4.0/>).

## 1. Introduction

Heavy rail steel mainly refers to rail with a nominal weight of 60–70 kg/m; thus, the material requires good impact strength, hardness, and wear resistance. Because inclusions in steel can cause internal damage to heavy rail steel and fatigue damage during use, the industry has placed strict requirements on the cleanliness of heavy rail steel; in particular, the control of inclusions in steel is extremely stringent [1–3]. According to the literature [4], research on 1080 MPa high-strength heavy rail steel showed that the addition of rare-earth elements in the steel can improve its wear resistance, corrosion resistance, strength, and other properties; thus, rare-earth heavy rail steel can be used as high-strength rail steel for applications in high-speed, heavy-haul railway transportation, as well as railway transportation with many curved sections. Compared with U75V, a heavy rail that does not contain rare earths, rare-earth heavy rail steel exhibits superior wear resistance, corrosion resistance, and impact toughness [5].

Rare-earth elements play a role in refining grains, modifying inclusions, and improving the cleanliness of steel [6,7]. Wang et al. [8] studied the control of Al<sub>2</sub>O<sub>3</sub> inclusions in high-strength IF steel-containing phosphorus. The results showed that when rare-earth Ce was added to the steel, the combination of Ce with the active O and S in the steel lowered the Gibbs free energy. In addition, CeAlO<sub>3</sub>, Ce<sub>2</sub>O<sub>2</sub>S, and Ce<sub>2</sub>O<sub>3</sub> could be generated easily, and composite rare-earth inclusions combined with other inclusions. The concentration and supersaturation of aluminium and oxygen decreased, and the ability of single particle Al<sub>2</sub>O<sub>3</sub> to aggregate into large-scale cluster inclusions reduced. The average size of Al<sub>2</sub>O<sub>3</sub> inclusions decreased from 5–7 μm to 2–5 μm in each thickness direction. The morphology of inclusions changed from the long strip, sharp angle, and cluster to the spherical, spindle,

and round surface. Meanwhile, the number density of  $\text{Al}_2\text{O}_3$  inclusions increased, but the area density decreased during the continuous casting and rolling process. Cheng et al. [9] studied the effect of rare earths on modifying inclusions in Al-killed X80 pipeline steel subjected to Ce treatment and found that Ce treatment modified and refined the inclusions. With the increase in Ce content from 0 wt.% to 0.025 wt.%, the mean size of inclusions first decreased from 2.41  $\mu\text{m}$  to 1.80  $\mu\text{m}$  and then increased to 1.87  $\mu\text{m}$ ; moreover, the proportion of inclusions smaller than 2  $\mu\text{m}$  gradually increased, while that of inclusions larger than 3  $\mu\text{m}$  initially decreased and then increased owing to the aggregation of Ce–O–S inclusions. The number density, largest size, and mean size of single MnS decreased after Ce treatment. Lan et al. [10] studied the effect of Ce treatment on nonmetallic inclusions in Fe–Mn–C–Al twinning-induced plasticity steel by adding different content of rare-earth cerium. Analyses showed that the main inclusions in Ce-treated steel change from  $\text{Al}_2\text{O}_3$ –MnS to  $\text{CeAlO}_3$ – $\text{Ce}_2\text{S}_3$ . With the increase in Ce content, the number, size, and density of inclusions in steel decreased, and the morphology of irregular inclusions was closer to the spindle. The size of inclusions in the test sample with 0.0048% Ce addition was the smallest, and the distribution of inclusions was the most uniform. The type, morphology, quantity, and size of inclusions in twinning-induced plasticity steel before and after Ce treatment. Meanwhile, combining the thermodynamic calculation results and experimental phenomena, the transformation path of the main inclusions in steel by Ce treatment is revealed. Wang et al. [11] studied the evolution and deformability of inclusions in steel containing rare-earth elements under different deoxidation conditions; the experiments under different deoxidation conditions were performed based on thermodynamic calculations in the Ce–Si–Al–O–S system, and the control conditions of various inclusions and the evolution of inclusions were investigated. The results show that  $\text{Al}_2\text{O}_3$  was modified to  $\text{CeAlO}_3$  with the addition of Ce and further transformed to  $\text{Ce}_2\text{O}_2\text{S}$  with the increase in Ce addition in Al-killed melts. The deformability of inclusions was improved by modifying  $\text{SiO}_2$ – $\text{Al}_2\text{O}_3$  to a  $\text{SiO}_2$ – $\text{Al}_2\text{O}_3$ – $\text{Ce}_2\text{O}_3$  inclusion. Among the rare-earth inclusions that are investigated in this study,  $\text{Ce}_2\text{SiO}_5$ , having a Young's modulus of less than 160 GPa, notably shows good deformability. Zhou et al. [12] studied the effect of Ce on the morphology of manganese sulphide, and we added different contents of Ce into U75V heavy rail steel. The composition and morphology of sulphide in steel were analysed. The number, size, and aspect ratio of the inclusions were analysed using the automatic scanning electron microscope ASPEX. The results show that the inclusions in heavy rail steel without Ce are elongated MnS and irregular Al–Si–Ca–O inclusions. With the increase of Ce from 52 ppm to 340 ppm, the composition of main inclusions changes along the route of  $\text{Ce}_2\text{O}_2\text{S}$ –MnS  $\rightarrow$   $\text{Ce}_2\text{O}_2\text{S}$ –MnS– $\text{Ce}_2\text{S}_3$   $\rightarrow$   $\text{Ce}_2\text{O}_2\text{S}$ – $\text{Ce}_3\text{S}_4$ – $\text{Ce}_2\text{S}_3$   $\rightarrow$   $\text{Ce}_2\text{O}_2\text{S}$ – $\text{Ce}_3\text{S}_4$ –CeS. Ce has a noticeable spheroidization effect on MnS, which can make inclusions finely dispersed. The average size of inclusions was the smallest when the Ce content was 139 ppm. The mechanism of Ce-modified MnS was discussed by combining experimental results with thermodynamic calculations. Finally, the effect of Ce treatment on inhibiting MnS deformation was verified by simulated rolling.

At present, few studies have reported on the industrial application of rare earths in steel, and the metamorphic mechanism of rare earths on the inclusions in steel is still unclear. Therefore, the effect of rare earths on the production of heavy rail steel urgently needs to be studied. In this study, the process of basic oxygen furnace (BOF)–ladle furnace (LF)–volume degassing (VD)–continuous casting (CC) in the industrial production of heavy rail steel is taken as the research object, and the action mechanism of rare-earth cerium on inclusions in steel is compared and analysed to provide a reference for the application of rare earths in heavy rail steel.

## 2. Materials and Methods

### 2.1. Test Materials

The chemical compositions of steels U75V and U76CrCe used in the smelting test are listed in Table 1. Ce content of added metal is [w(Ce) > 99.9%].

**Table 1.** Chemical composition of steel billet samples used in the test (mass fraction) %.

Steel Grade	$w_B/\%$										
	C	Si	Mn	P	S	V	Cr	Al	Re	O	Fe
U75V	0.75	0.55	0.79	0.014	0.008	0.005	0	0.0035	0	0.0014	balance
U75V	0.72	0.60	0.81	0.010	0.012	0.005	0	0.0031	0	0.0018	balance
U75V	0.71	0.59	0.77	0.011	0.011	0.004	0	0.0045	0	0.0017	balance
U75V	0.74	0.56	0.79	0.010	0.005	0.006	0	0.0041	0	0.0018	balance
U76CrRe	0.79	0.69	0.94	0.016	0.003	0.048	0.0724	0.0028	0.0085	0.0015	balance
U76CrRe	0.79	0.73	0.97	0.017	0.001	0.042	0.0765	0.0034	0.0091	0.0016	balance
U76CrRe	0.79	0.67	0.93	0.015	0.002	0.043	0.0772	0.0028	0.0083	0.0012	balance
U76CrRe	0.80	0.68	0.94	0.014	0.001	0.051	0.0786	0.0029	0.0084	0.0018	balance

## 2.2. Test Scheme

In this study, the field production process of heavy rail steel in China, which involved the use of a BOF and LF, as well as the VD and CC processes, was investigated. An experimental scheme of Ce addition for heavy rail steel was designed. The capacity of the smelting test steel converter is 150 t; in off-furnace refining, an LF is used for deoxidising and alloying liquid steel. The settings for the VD refining furnace were as follows: vacuum < 8 KPa, deep vacuum time > 15 min; the cross-section of the billet was 280 mm × 380 mm, and the fixed size was 7.72 m. Metal Ce (0.45 kg/t Ce per t of Fe) was added after the molten steel was subjected to VD refining. Soft-blowing and static measures were used to ensure that the inclusions could fully grow and float after the Ce reaction. The billet sample was obtained from the cut surface of the billet. The Ce contents of all billet samples were evaluated using chemical analysis, and the quantity and size of the inclusions in the samples were analysed and compared with those of U75V without Ce. To avoid errors, four furnace heavy rail steels U75V and rare-earth heavy rail steels U76CrCe were randomly selected for analysis and statistical analysis, and the average value was subjected to comparative analysis.

## 2.3. Detection Method

### 2.3.1. Low-Multiplier Detection of Inclusions in Steel

The fourth rail of each of the 4 stoves of U75V and U76CrCe works was cut in a cross-section 100 mm from the rail head. A total of 8 10 mm × 10 mm × 5 mm samples were obtained from the top of the rail. The surface of the sample parallel to and facing the central axis of the rail was polished using a diamond abrasive, and the inclusions in the polished surface were observed using a Zeiscale Axioscope (Germany) electron microscope at 100× with an area of 0.5 mm<sup>2</sup> at minimum for each sample. The conditions of the inclusions were observed and recorded, and 104 low-power inclusion detection images were obtained.

### 2.3.2. Scanning Electron Microscopy–Energy-Dispersive X-ray Spectroscopy (SEM-EDS) Analysis

Four U75V and U76CrCe samples were obtained from the tail of the third cast billet at the second flow of each test furnace. Then, 10 mm × 10 mm × 5 mm cast billet samples were obtained from a quarter of the distance away from the side of the cast billet. The samples were polished step-by-step using metallographic sandpaper to 1200# to obtain a scratch-less surface. The samples were placed in a beaker containing ethanol with or without water, cleaned using an ultrasonic cleaning instrument, and finally dried using a high-pressure gun prior to use. Using a Zeiscale SIGMA-300 (Germany) field emission scanning microscope equipped with energy dispersive X-ray spectroscope, the samples were analysed by SEM-EDS in multiple fields under an accelerating voltage of 20 keV and accelerating current of 1.0 nA. Simultaneously, photographs of the typical inclusions in the sample were obtained, and the distribution of elements in the inclusions was analysed by EDS. The size and composition of each inclusion detected in the multi-field of view were

analysed statistically. The scanning area of the multi-field of view detection was 11.56 mm<sup>2</sup>; a total of 1760 inclusions were detected.

### 3. Thermodynamic Calculations

When the rare-earth elements react with the impurities such as O and S in the steel, inclusions such as cerium oxides, sulphides, sulphur oxides, and aluminates are formed at a production temperature of 1873 K. The Gibbs free energies of Ce reacting with the elements in liquid steel are shown in Table 2, and the interaction coefficients of the elements in liquid steel are listed in Table 3.

**Table 2.** Gibbs free energies of the reactions involving La and Ce inclusions (J/mol).

Reaction Formula	$\Delta G^0$	$\Delta G$ (1873 K)
$[\text{Ce}] + 3/2[\text{O}] = 1/2\text{Ce}_2\text{O}_3$	$-714,380 + 179.74T$	$-377,726.98$
$[\text{Ce}] + [\text{O}] + 1/2[\text{S}] = 1/2\text{Ce}_2\text{O}_2\text{S}$	$-675,700 + 165.50T$	$-365,718.50$
$[\text{Ce}] + 3/2[\text{S}] = 1/2\text{Ce}_2\text{S}_3$	$-536,420 + 163.86T$	$-229,510.22$
$[\text{Ce}] + 4/3[\text{S}] = 1/3\text{Ce}_3\text{S}_4$	$-497,670 + 146.30T$	$-223,650.10$
$[\text{Ce}] + [\text{S}] = \text{CeS}$	$-422,100 + 120.38T$	$-196,628.26$
$[\text{Ce}] + 3[\text{O}] + [\text{Al}] = \text{CeAlO}_3$	$-1,366,460 + 364.30T$	$-684,126.10$
$[\text{Mn}] + [\text{S}] = \text{MnS}$	$-39,469 + 21.71T$	$1193.83$

**Table 3.** Interaction coefficients of elements in liquid steel at 1873 K.

	C	Si	Mn	P	Al	O	S	Ce
O	−0.45	−0.131	−0.021	0.07	−3.9	−0.02	−0.133	−0.57
S	0.122	0.063	−0.026	0.029	0.035	−0.27	−0.026	−
Ce	−	−	−	−	−	−5.03	−	−
Al	0.091	0.0056	0.035	0.033	0.045	−6.6	0.03	−

The Gibbs free energy of the reaction at different temperatures can be calculated using Equations (1)–(3).

$$\Delta G = \Delta G^0 + RT \ln Q \quad (1)$$

$$\lg f_i = \sum_j^n e_i^j \omega(j) \quad (2)$$

$$a_i = f_i \cdot \omega(i) \quad (3)$$

In these equations,  $\Delta G$  is the Gibbs free energy,  $\Delta G^0$  is the Gibbs free energy at the same temperature and standard pressure,  $R$  is the gas constant,  $T$  is the thermodynamic temperature,  $Q$  is the reaction entropy,  $f_i$  is the activity coefficient of substance  $i$ ,  $a_i$  is the activity of substance  $i$ ,  $\omega(i)$  and  $\omega(j)$  are the mass fractions of  $i$  and  $j$ , respectively, and  $e_{ij}$  is the activity interaction coefficient of  $i$  and  $j$ .

As seen from the thermodynamic analysis of possible inclusion formation in steel at the Ce addition temperature of 1873 K, compared with oxides, sulphides, and sulphur oxides of Ce, the Gibbs free energy of  $\text{CeAlO}_3$  generation is lower, indicating that  $\text{CeAlO}_3$  is most easily generated by Ce under the composition and temperature conditions of the liquid steel. According to the possible products of Ce in steel and the activity of each element, when wt. [%Ce] content is less than 0.01,  $\text{CeAlO}_3$ ,  $\text{Ce}_2\text{O}_3$ ,  $\text{Ce}_2\text{O}_2\text{S}$ , and  $\text{CeO}_2$  are formed in the liquid steel successively. Based on the Ce content shown in Table 1, it is inferred that  $\text{CeAlO}_3$  is most easily formed when 0.45 kg/t Ce is added to the heavy rail steel.

## 4. Results

### 4.1. Effect of Ce on Inclusions in Heavy Rail Steel

Figure 1 shows the low-multiplier analysis of the typical inclusions in U75V and U76CrCe cast billet samples.

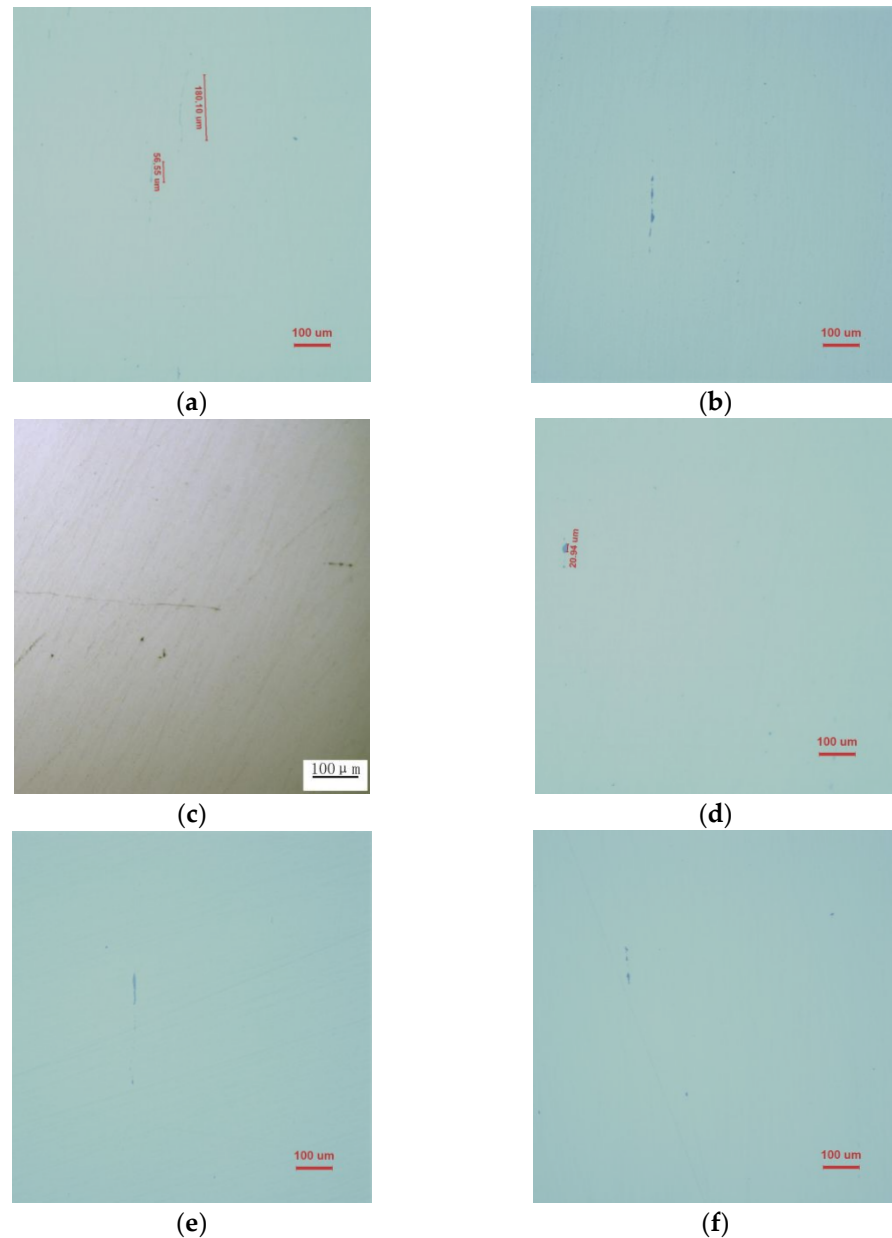


**Figure 1.** Electron microscopy analysis results of the rail samples U75V and U76CrCe: (a) class A inclusion in U75V; (b) class B inclusion in U75V; (c) class D inclusion in U75V; (d) class Ds inclusion in U75V; (e) class A inclusion in U76CrCe; and (f) class B inclusion in U76CrCe.

As can be seen from Figure 1, category A, B, D, and Ds inclusions are the main inclusions in the U75V cast billet samples. The size of inclusions in the U76CrCe cast billet samples decreased significantly. D and Ds inclusions disappeared, and the number of A inclusions decreased considerably. The B inclusions changed from continuous droplets to discontinuous few droplets or individually distributed particles. Therefore, the addition of Ce was effective in improving the cleanliness of the casting billet and reducing the number and size of inclusions in steel.

Figures 2 and 3 show the microstructure changes of the aluminium-containing inclusions in the U75V and U76CrCe cast billet samples.

As seen from Figure 2, the aluminium inclusion in the U75V cast billet samples without rare-earth addition includes  $\text{CaO-MgO-Al}_2\text{O}_3\text{-SiO}_2$  (Figure 2a), while that in U76CrCe billet samples is mainly  $\text{CaO-MgO-Al}_2\text{O}_3\text{-SiO}_2\text{-CeO}$  inclusion (Figure 2b). When added to steel, Ce mainly reacts with  $\text{CaO-MgO-Al}_2\text{O}_3\text{-SiO}_2$  to form  $\text{CaO-MgO-Al}_2\text{O}_3\text{-SiO}_2\text{-CeO}$ . The distribution of Ce and aluminium was coincident, indicating that Ce mainly reacted with aluminium in steel. The addition of Ce changed the shape of the aluminium inclusion from an irregular shape to a circular shape, which consequently improved the stress concentration caused by the inclusion of  $\text{CaO-MgO-Al}_2\text{O}_3\text{-SiO}_2$  in U75V and helped to improve the performance of heavy rail steel. Meanwhile, S was enriched on the surface of  $\text{CaO-MgO-Al}_2\text{O}_3\text{-SiO}_2\text{-CeO}$ .

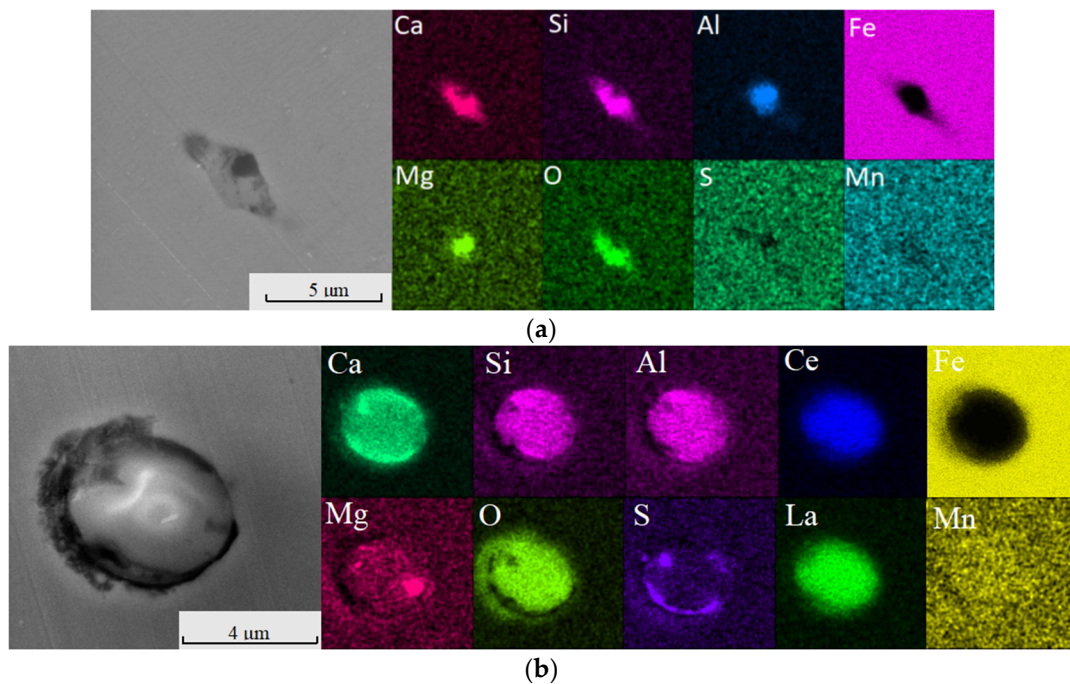


**Figure 2.** Photographs and EDS analysis results of inclusions in U75V and U76CrCe cast billet samples. (a) Photographs and EDS analysis results of the  $\text{CaO-MgO-Al}_2\text{O}_3\text{-SiO}_2$  inclusions in U75V cast billet samples, and (b) photographs and EDS analysis results of  $\text{CaO-MgO-Al}_2\text{O}_3\text{-SiO}_2\text{-CeO}$  inclusions in U76CrCe cast billet samples.

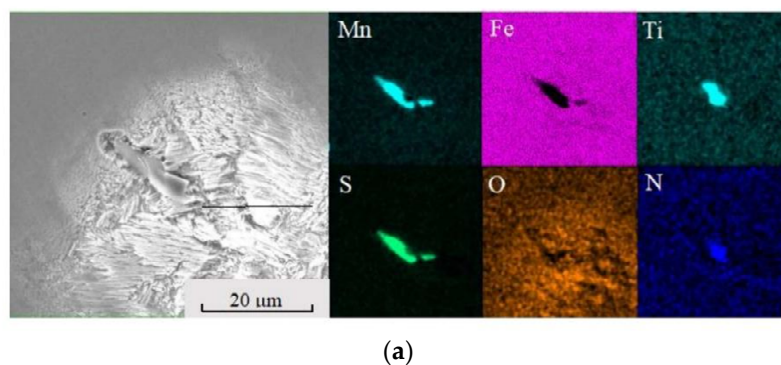


**Figure 3.** Cont.

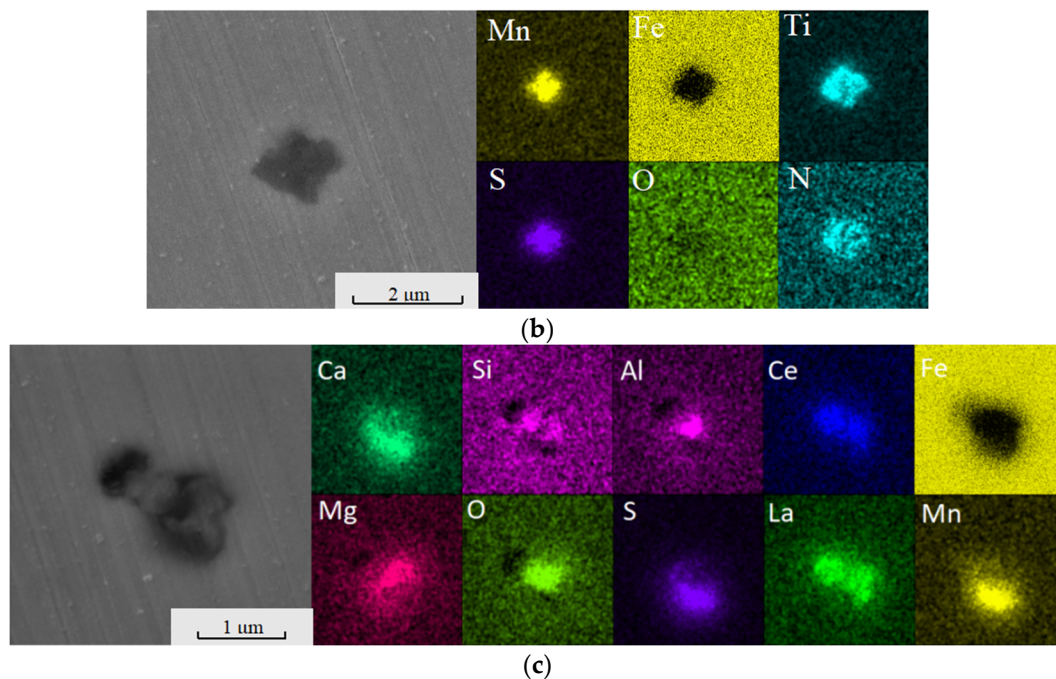


**Figure 3.** Photographs and EDS analysis results of inclusions in U76CrCe cast billet samples. (a) Photographs and EDS analysis results of MnS inclusions in U75V cast billet samples; (b) photographs and EDS analysis results of MnS inclusions in U76CrCe cast billet samples; and (c) photographs and EDS analysis results of CaO–MgO–Al<sub>2</sub>O<sub>3</sub>–SiO<sub>2</sub>–CeO and MnS composite inclusions in U76CrCe cast billet samples.

As seen in Figure 3, the sulphide in the cast billet samples is mainly present in the MnS inclusions. The figure also shows the microstructure changes of sulphide inclusions in the cast billet samples. The addition of Ce considerably reduced the size of MnS inclusions in the cast billet samples; most of the MnS inclusions changed from the long shape (Figure 3a) to polygonal with low length and width (Figure 3b), and most of the MnS inclusions were dispersion distribution. Meanwhile, more CaO–MgO–Al<sub>2</sub>O<sub>3</sub>–SiO<sub>2</sub>–CeO and MnS formed complex inclusions (Figure 3c). The reduction in size and appearance of composite inclusions can reduce the probability of forming elongated inclusions during the rolling process of MnS inclusions, thereby reducing the phenomenon of stress concentration around MnS inclusions and improving the comprehensive performance of heavy rail steel.

Figure 4 shows the statistical results of inclusion size in U75V and U76CrCe cast billet samples investigated using SEM multi-field analysis.

As shown in Figure 4, the densities of inclusions in the U75V and U76CrCe cast billet samples are 88.27 and 78.70 particles/mm<sup>2</sup>, respectively. The length of inclusions mainly ranged from 1 μm to 5 μm, and the density of inclusions greater than 5 μm decreased considerably. The length of inclusions in length less than 1 μm, and between 1 and 5 μm, increased from 5.63 and 61.26/mm<sup>2</sup> in U75V samples to 7.38 and 64.46/mm<sup>2</sup> in U76CrCe samples, the inclusions density decreased in length between 5 and 10 μm, between 10 and 20 μm from 13.76 and 6.28 particles/mm<sup>2</sup> in the U75V samples to 4.95 and 1.91 particles/mm<sup>2</sup> in the U76CrCe samples correspondingly. No inclusions exceeding 20 μm in length were found in the U76CrCe samples. The change in the size distribution of inclusions in steel indicates that the addition of Ce can promote the dispersion degree of inclusions in steel.

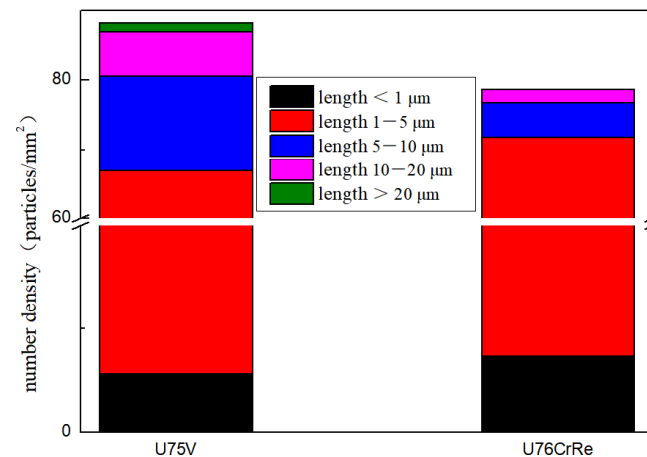


**Figure 4.** Statistical results of inclusion density distribution in cast billet samples of U75V and U76CrCe.

#### 4.2. Effect of Ce in Heavy Rail Steel on Aluminium Inclusion

To further analyse the influence of Ce on aluminium-containing inclusions in heavy rail steel, multi-field scanning results show that the density and length of inclusions in samples were statistical, as shown in Figure 5.

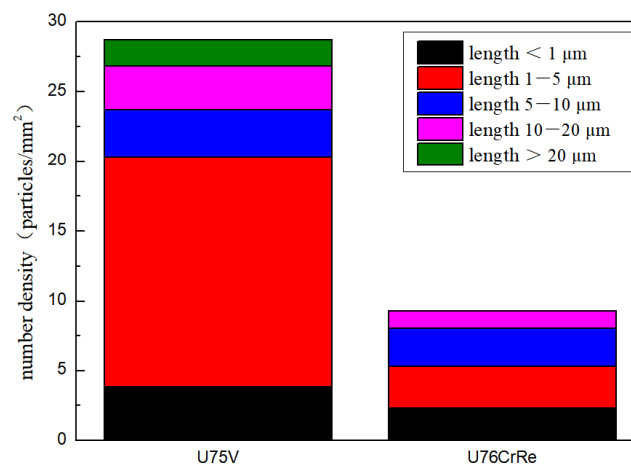


**Figure 5.** Statistical results of the different density distribution of aluminium inclusions density in U75V and U76CrCe cast billet samples.

As shown in Figure 5, under the action of Ce, the number density of aluminium-containing inclusions in the samples decreases from 28.72 particles/mm<sup>2</sup> in U75V to 9.33 particles/mm<sup>2</sup> in U76CrCe. The number density of inclusions with lengths between 1 and 5 µm decreased the most from 16.43 particles/mm<sup>2</sup> in U75V to 3 particles/mm<sup>2</sup> in U76CrCe. The number density of aluminium-containing inclusions with lengths less than 1 µm, between 5 and 10 µm, and between 10 and 20 µm decreased from 3.87, 3.42, and 3.11 particles/mm<sup>2</sup> to 2.33, 2.67, and 1.33 particles/mm<sup>2</sup>, respectively. The number density of inclusions between 1 and 5 µm decreased significantly, while that in the other length ranges also decreased to different degrees. No aluminium-containing inclusions greater than 20 µm in length were found in the U76CrCe samples.

The melting point of Ce metal and the solid solution in iron were extremely low. When Ce was added to liquid steel at 1800 K, it first melted into a liquid and existed in the form of a dispersion in the liquid steel. Under argon stirring conditions, the liquid Ce reacted with Al<sub>2</sub>O<sub>3</sub> (melting point 2327.15 K) particles in the molten steel. The reaction conforms to the transition state theory, and the reaction was carried out through the following steps:

- (1) Liquid Ce was enriched at the interface between solid  $\text{Al}_2\text{O}_3$  and liquid steel;
- (2) Ce diffused from the interface to the  $\text{Al}_2\text{O}_3$  interior;
- (3) Reaction:  $[\text{Ce}] + 3[\text{O}] + [\text{Al}] = \text{CeAlO}_3$ ;
- (4) The solid  $\text{CeAlO}_3$  generated by the reaction wrapped the unreacted  $\text{Al}_2\text{O}_3$  and the unreacted Ce diffused to the  $\text{Al}_2\text{O}_3$  through the  $\text{CeAlO}_3$  layer to continue the reaction, and the reaction occurred at the interface between  $\text{Al}_2\text{O}_3$  and  $\text{CeAlO}_3$ .
- (5)  $\text{CeAlO}_3$  particles were formed after the reaction between  $\text{Al}_2\text{O}_3$  and Ce.

According to the reaction between  $\text{Al}_2\text{O}_3$  and Ce, owing to the larger atomic radius of the Ce atom ( $1.842 \times 10^{-10}$  m) than that of the Al atom ( $1.429 \times 10^{-10}$  m), the Ce atom entered the  $\text{Al}_2\text{O}_3$  lattice during the reaction and destroyed the original crystal structure, which was represented by an increase in volume from a macroscopic perspective. During the above steps (3) to (4), the generated  $\text{CeAlO}_3$  broke off at the sharp corners, and the narrow parts of the  $\text{Al}_2\text{O}_3$  particles formed numerous small, irregularly shaped particles owing to expansion. The above process repeated until smaller spherical  $\text{CeAlO}_3$  particles were formed. A stable spherical  $\text{CeAlO}_3$  shell of the inclusion particle was formed on the particle surface. Subsequently, the unreacted  $\text{Al}_2\text{O}_3$  inside the particle reacted with the Ce outside the  $\text{CeAlO}_3$  shell through diffusion, thereby leading to the formation of spherical  $\text{CeAlO}_3$  particles.

Figure 6 shows a schematic diagram of the reaction process of Ce to Al inclusion in steel.

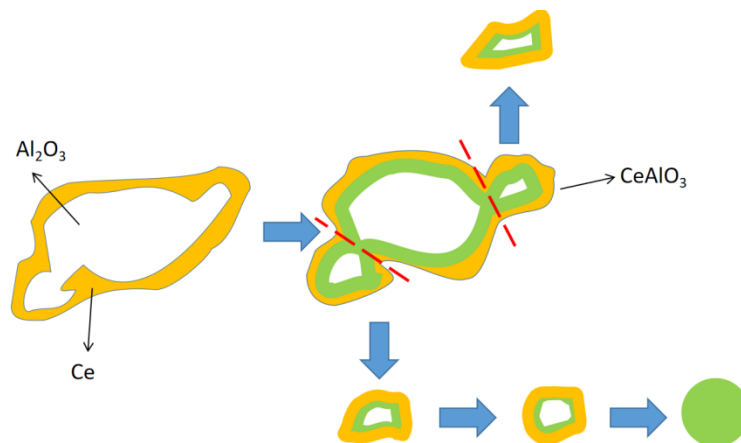


**Figure 6.** Schematic diagram of the reaction process of alumina and metal cerium.

The smaller the inclusion size, the lower its ability to condense and the poorer its ability to aggregate and grow [13–15]. The collision probability mainly involves Brown, Stokes, and turbulent collision. The decrease in reaction concentration, nucleation number, and inclusion size can directly affect the collision times of inclusions and reduce the growth ability of inclusions. The smoother the surface morphology of the inclusions is, the smaller the shape coefficient of the particles and resistance to floating is, and the easier it is for the inclusions to float.

Therefore, aluminium inclusions in heavy rail steel react under the action of Ce to form  $\text{CeAlO}_3$ , which are small, circular-shaped inclusions. Solid  $\text{CeAlO}_3$  inclusions are difficult to aggregate and grow and easy to float and remove. Therefore, the addition of Ce can effectively reduce the size and quantity of aluminium inclusions in heavy rail steel.

#### 4.3. Effect of Ce in Sulphide Inclusion in Heavy Rail Steel

The number and length of sulphide inclusions in U75V and U76CrCe cast billet samples were analysed using SEM and EDS, as shown in Figure 7.

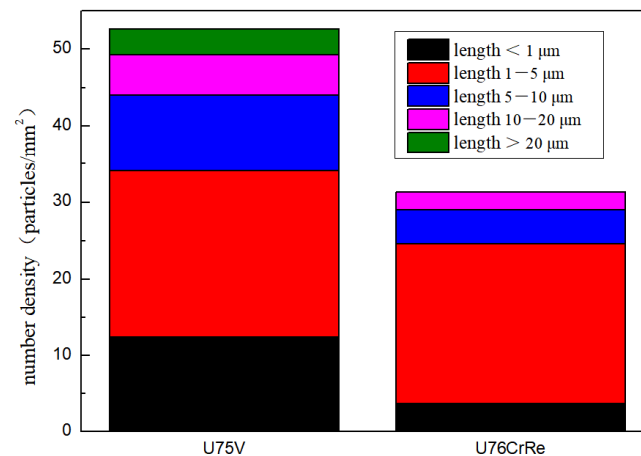


**Figure 7.** Statistical results of different sizes of density distribution of sulphide inclusions in U75V and U76CrCe cast slab samples.

As seen in Figure 7, the addition of Ce reduced the number density of sulphide inclusions in heavy rail steel from 52.7 particles/mm<sup>2</sup> to 31.33 particles/mm<sup>2</sup>. The densities of inclusions with lengths less than 1 µm, between 1 and 5 µm, between 5 and 10 µm, and between 10 and 20 µm decreased from 12.4, 21.7, 10, and 5.2 particles/mm<sup>2</sup> to 3.67, 21, 4.33, and 2.33 particles/mm<sup>2</sup>, respectively. The number density of inclusions between 5 and 20 µm decreased significantly, while the number density of inclusions in other length ranges decreased to different degrees. The number density of inclusions larger than 20 µm decreased to 0 particles/mm<sup>2</sup>.

In this research system, sulphur compounds in heavy rail steel are mainly the MnS inclusions. It can be seen from Figure 8 that the Gibbs free energy of Ce combined with S in steel is much lower than that of Mn combined with S. Therefore, solid-solution element S in liquid steel first reacts with Ce to form sulphide or sulphur oxide inclusions, which decrease the concentration of S in liquid steel. When the temperature of liquid steel decreases to the MnS precipitation temperature, the concentration of S in steel decreases. The decrease in precipitation of MnS resulted in a decrease in the size and quantity of MnS inclusions. Meanwhile, because the precipitation of MnS primarily occurs on the surface of other inclusions, typical MnS inclusions coated by MnS are formed. With the action of Ce, the number and size of aluminium inclusions in steel decreased, along with the size and quantity of MnS inclusions. A comparative analysis of the typical aluminium-containing inclusion in U75V and the aluminium-containing inclusion in U76CrCe revealed that S precipitated easily and attached to the surface of the inclusion during the solidification process of U76CrCe, increasing the precipitation probability of MnS on the surface. Consequently, CaO–MgO–Al<sub>2</sub>O<sub>3</sub>–SiO<sub>2</sub>–CeO and MnS composite inclusions easily formed. Compared with the long-strip MnS inclusions, the composite inclusions were more rounded in shape and easier to float and remove; thus, the number of MnS inclusions in steel decreased accordingly.

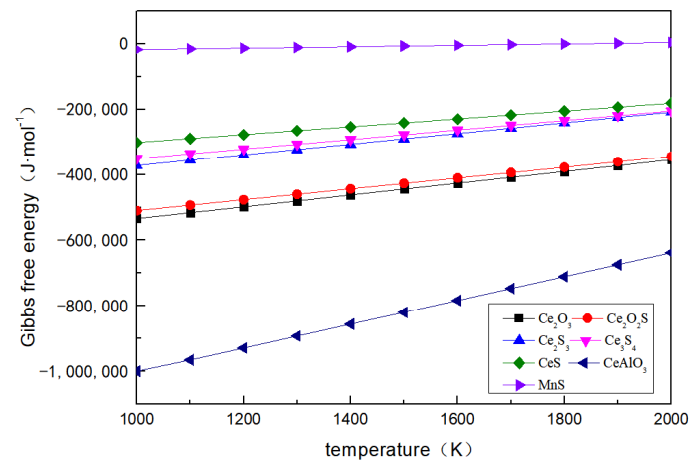


**Figure 8.** Thermodynamic analysis of possible inclusion formation in molten steel.

## 5. Conclusions

- (1) Under the test conditions, the addition of Ce can effectively reduce the number and size of class A and B inclusions in the cast billet samples and make class D and Ds inclusions completely disappear in heavy rail steel. Meanwhile, the CaO–MgO–Al<sub>2</sub>O<sub>3</sub>–SiO<sub>2</sub> inclusions change from irregularly shaped to round, and the MnS inclusions change in shape from long strips to squares with similar lengths and widths.
- (2) Multi-field analysis shows that the addition of Ce can effectively reduce the number density and size of inclusions in heavy rail steel; in particular, inclusions longer than 5  $\mu\text{m}$  decreased significantly, while those shorter than 5  $\mu\text{m}$  increased, indicating that Ce can promote the dispersion distribution of inclusions in heavy rail steel.
- (3) Under these test conditions, the aluminium-containing inclusions were converted into smaller spherical CeAlO<sub>3</sub> inclusions after the addition of Ce, which can reduce the collision growth probability of such inclusions and simplify their floating and removal. The number density of aluminium inclusions in steel decreased from 28.72 particles/mm<sup>2</sup> to 9.33 particles/mm<sup>2</sup>. The size distribution of aluminium inclusions changed: the number density of aluminium inclusions with the length of 1–5  $\mu\text{m}$  decreased from 16.43 particles/mm<sup>2</sup> to 3 particles/mm<sup>2</sup>, while those of other length inclusions also decreased to different degrees.
- (4) Under the experimental conditions, Ce reacted with the solid solution [S] in the liquid steel to reduce the [S] concentration in the liquid steel, which aided the reduction in the number and size of the inclusion core required for the growth of MnS inclusions in steel; meanwhile, CaO–MgO–Al<sub>2</sub>O<sub>3</sub>–SiO<sub>2</sub>–CeO and MnS composite inclusions were formed more. Thus, the number density of MnS inclusions in steel decreased from 52.7 particles/mm<sup>2</sup> to 31.33 particles/mm<sup>2</sup>, and the size distribution of MnS inclusions changed. The number density of inclusions with lengths between 5 and 10, lengths between 10 and 20, and larger than 20  $\mu\text{m}$ , which showed the most obvious change, decreased from 12.4, 21.7, 10, and 5.2 particles/mm<sup>2</sup> to 4.33, 2.33, and 0 particles/mm<sup>2</sup>, respectively.

**Author Contributions:** Conceptualization, G.B. and J.Y.; methodology, G.B.; software, G.B. and W.L.; validation, G.B., J.Y., and W.L.; formal analysis, G.B. and W.L.; investigation, G.B. and W.L.; resources, J.Y.; data curation, G.B. and W.L.; writing—original draft preparation, G.B. and W.L.; writing—review and editing, G.B. and J.Y.; visualization, G.B. and W.L.; supervision, J.Y.; project administration, J.Y.; funding acquisition, J.Y. All authors have read and agreed to the published version of the manuscript.

**Funding:** This research was funded by the National Natural Science Foundation of China, grant number 51774190.

**Data Availability Statement:** The authors declare that all data is available upon request.

**Acknowledgments:** We are grateful for support from the National Natural Science Foundation of China (grant number 51774190), the School of Materials and Metallurgy at Inner Mongolia University of Science & Technology, and Inner Mongolia Autonomous Region Rare Earth Steel Product R&D Enterprise Key Laboratory of Baotou Steel, China.

**Conflicts of Interest:** The authors declare no conflict of interest.

## References

1. Belalia, A.; Kamla, Y.; Amara, M.; Hadj Meliani, M.; El Azizi, A.; Azari, Z. Experimental and numerical investigation of UIC 54 rail degradation. *Eng. Fail. Anal.* **2020**, *111*, 104163. [[CrossRef](#)]
2. Kormyshev, V.E.; Gromov, V.E.; Ivanov, Y.F.; Glezer, A.; Yuriev, A.A.; Semin, A.P.; Sundeev, R.V. Structural phase states and properties of rails after long-term operation. *Mater. Lett.* **2020**, *268*, 127499. [[CrossRef](#)]
3. Jing, J.L.; Ya, F.G.; Yue, S.W.; Chang, H.Y. Experimental Research on Crack Propagation in U71Mn and U75V Rail Steels. *Key Eng. Mater.* **2006**, *43*, 807–810.
4. Wang, H.; Bao, Y.; Duan, C.; Lu, L.; Liu, Y.; Zhang, Q. Effect of Rare Earth Ce on Deep Stamping Properties of High-Strength Interstitial-Free Steel Containing Phosphorus. *Materials* **2020**, *13*, 1473. [[CrossRef](#)] [[PubMed](#)]
5. Li, D.; Wang, P.; Chen, X.-Q.; Fu, P.; Luan, Y.; Hu, X.; Liu, H.; Sun, M.; Chen, Y.; Cao, Y.; et al. Low-oxygen rare earth steels. *Nat. Mat.* **2022**, *21*, 1137–1143. [[CrossRef](#)] [[PubMed](#)]
6. Bao, X.R.; Wang, J.A.; Wang, X.D.; Guo, F.; Liu, Y. Effects of lanthanum on hot deformation behaviour of Mn-Cr-Mo bainitic rail steel. *J. Rare Earths* **2018**, *36*, 772–780. [[CrossRef](#)]
7. Xu, Y.W.; Song, S.H.; Wang, J.W. Effect of rare earth cerium on the creep properties of modified 9Cr-1Mo heat-resistant steel. *Mater. Lett.* **2015**, *161*, 616–619. [[CrossRef](#)]
8. Wang, H.; Bao, Y.P.; Zhi, J.G.; Duan, C.-y.; Gao, S.; Wang, M. Effect of Rare Earth Ce on the Morphology and Distribution of Al<sub>2</sub>O<sub>3</sub> Inclusions in High Strength IF Steel Containing Phosphorus during Continuous Casting and Rolling Process: Fundamentals of High Temperature Processes. *ISIJ Int.* **2021**, *61*, 657–666. [[CrossRef](#)]
9. Cheng, W.S.; Song, B.; Yang, Z.B.; Mao, J. Effect of Rare Earth Ce on Modifying Inclusions in Al-killed X80 Pipeline Steel. *Trans. Indian Inst. Met.* **2022**, *75*, 2837–2846. [[CrossRef](#)]
10. Lan, F.-J.; Zhuang, C.-L.; Li, C.-R.; Yang, H.; Yang, G.-K.; Yao, H.-J.; Zhang, Z.-Z. Effect of Rare-Earth Cerium on Nonmetallic Inclusions in Fe–Mn–C–Al Twinning-Induced Plasticity. *Steel. Steel Res. Int.* **2022**, *94*, 2200421. [[CrossRef](#)]
11. Wang, Y.G.; Liu, C.J. Evolution and Deformability of Inclusions in Steel Containing Rare-Earth Element Under Different Deoxidation Conditions. *Steel. Steel Res. Int.* **2022**, *93*, 2200027. [[CrossRef](#)]
12. Zhuo, C.; Liu, R.; Zhao, Z.; Zhang, Y.; Hao, X.; Wu, H.; Sun, Y. Effect of Rare Earth Cerium Content on Manganese Sulfide in U75V Heavy Rail Steel. *Metals* **2022**, *12*, 1012. [[CrossRef](#)]
13. Lin, Q.; Guo, F.; Zhu, X.Y. Behaviors of Lanthanum and Cerium on Grain Boundaries in Carbon Manganese Clean Steel. *J. Rare Earths* **2007**, *25*, 485–489. [[CrossRef](#)]
14. Yu, Y.C.; Chen, W.Q.; Zhen, H.G. Effect of Cerium and Mischmetal on Solidification Structure of Fe-36Ni Low Expansion alloy. *J. Chin. Soc. Rare Earths* **2012**, *30*, 175–180.
15. Huang, Y.; Cheng, G.G.; Xie, Y. Modification Mechanism of Cerium on the inclusions in Drill Steel. *Acta Metall. Sin.* **2018**, *54*, 1253–12661.

**Disclaimer/Publisher’s Note:** The statements, opinions and data contained in all publications are solely those of the individual author(s) and contributor(s) and not of MDPI and/or the editor(s). MDPI and/or the editor(s) disclaim responsibility for any injury to people or property resulting from any ideas, methods, instructions or products referred to in the content.